International Journal of Remote Sensing
Vol. 31, No. 19, 10 September 2010, 5041–5059

Taylor & Francis
Taylor & Francis Group

Straight road edge detection from high-resolution remote sensing images based on the ridgelet transform with the revised parallel-beam Radon transform

XIAOFENG LI†‡, SHUQING ZHANG*†, XIN PAN†‡, PAT DALE§ and ROGER CROPP§

†Northeast Institute of Geography and Agricultural Ecology, Chinese Academy of Sciences, Changchun, 130012, China

‡Graduate University of the Chinese Academy of Sciences, Beijing, 100039, China

§Griffith School of Environment, Griffith University, Nathan, QLD 4111, Australia

(*Received 31 May 2007; in final form 12 November 2008*)

Roads are important basic geographical phenomena and the automatic recognition and extraction of road features from remote sensing images has many applications. However, automated road extraction from high-resolution remote sensing imagery is problematic. In recent years, many approaches have been explored for automatic road extraction, particularly involving road edge detection. Traditional edge detection operators such as the Canny or the Sobel operator are used frequently but there are serious problems of over- or underdetection, and time-consuming and complicated post-processing work is often required. In this paper, a new revised parallel-beam Radon transform (RPRT) approach is proposed. The traditional PRT can have problems with step values, resulting in false edge detection. To overcome these problems we introduced the RPRT, using the harmonic average of the pixel value in every strip of the Radon slice. An algorithm suitable for straight edge detection of roads in high-resolution remote sensing imagery was designed based on the ridgelet transform with the RPRT. The experimental results show that our algorithm can detect straight road edges efficiently and accurately, and avoid cumbersome and complicated post-processing work.

1. Introduction

With the development of high-resolution remote sensing imagery such as IKONOS and QuickBird, automatic rapid and accurate extraction of information from imagery of man-made objects (e.g. roads and buildings) is an important issue relevant to planning and management. Roads are important geographical features, so methods for their automatic recognition and extraction are applicable in many areas such as updating geographical information, image interpretation and mapping at a large scale (Guan *et al.* 2006). However, automated road extraction from high-resolution remote sensing imagery is problematic because the relatively small details, such as shadows, trees along streets or vehicles on lanes, can disturb the numerical processes of road network extraction (Couloigner and Ranchin 2000).

In recent years, many approaches have been developed for road extraction from imagery. According to Mena (2003), road extraction techniques can be broadly

*Corresponding author. Email: shqzhang@263.net

International Journal of Remote Sensing
ISSN 0143-1161 print/ISSN 1366-5901 online © 2010 Taylor & Francis
http://www.tandf.co.uk/journals
DOI: 10.1080/01431160903283835

divided into 'mid- and high-level methods' and 'low- and mid-level methods'. The mid- and high-level methods seek an analysis and interpretation of the image similar to that of a human operator. However, better implementation of mid- and high-level methods requires solid knowledge derived from low- and mid-level methods.

The low- and mid-level methods include 'road tracking', 'morphology and filtrate', 'dynamic programming and snakes', 'multi-scale and multi-resolution' and 'segmentation and classification'. Many of these methods are relevant to road edge detection. Among the road tracking methods, for example, Nevatia and Babu (1980) and Dal Poz *et al.* (2000) considered edge detection and analysis. Based on edge detection and filter usage, several morphology and filtrate road extraction approaches have been explored (e.g. Oliveira and Caeiro 2000, Chiang *et al.* 2001). In the dynamic programming and snakes methods, Laptev *et al.* (2000) proposed an approach for automatic road extraction from aerial imagery with geometry constrained edge extraction using 'snakes'. Edges may also be detected by means of texture analysis for road extraction at multi-scales and multi-resolutions (e.g. Hinz *et al.* 2001).

Methods for edge detection have been studied intensively, and a large number of operators have been invented (e.g. the Canny, Sobel and Roberts operators). However, these traditional edge detectors based on the per-pixel value difference are inefficient when applied to road edge detection. Many non-road edges are often detected by these operators. Edge pixels extracted by operators such as the Canny filter and the Sobel edge detector reflect not only the boundaries of roads but also those of buildings, rivers or shadows and any other local rapid changes of photometric characteristics (Touzi *et al.* 1988). Therefore, time-consuming and complicated post-processing work is often needed.

Wavelets, as one of the tools of multi-resolution analysis (MRA), have been widely used in edge detection (e.g. Mallat and Zhong 1992, Li and Shao 1994, Schmeelk 2005). However, two-dimensional (2D) wavelets, usually extended by 1D wavelets (i.e. separable wavelets), are far from efficient in representing edges in images because of the inability to encompass multi-orientation transforms. Multi-orientation (not only horizontal or vertical) is an important geometric characteristic that is particularly useful for road edge detection in remote sensing imagery. The ridgelet transform is another extension of wavelets to two dimensions that is better than Fourier and wavelet transforms for approximating functions with singularities along lines because of its multi-orientation transform. In fact, the ridgelet transform can be explained as the application of wavelets to the Radon domain (Candès and Donoho 1999, Donoho 2000, Ramos Terrades and Valveny 2006). Constructing the ridgelet transform effectively by improving the Radon transform and letting it better combine wavelets is self-evidently important.

The Radon transform is an integral transform consisting of the integral of a function over straight lines and was first put forward by Johann Radon (Radon 1917). In the past two decades, substantial work has been completed to improve the quality of Radon transform-based linear feature detectors (Zhang and Couloiger 2007). For example, Copeland *et al.* (1995) modified the Radon transform so as to localize the area in which each integration takes place. Du and Yeo (2004) developed a novel method for detecting ship wakes in synthetic aperture radar (SAR) images based on the gliding-box algorithm and the Radon transform algorithm. Zhang and Couloiger (2007) proposed a mean filter to locate the true peak in the Radon image and used a profile analysis technique to further refine the line parameters. Aiming at linear feature extraction rather than edge detection, however, these methods are not

suitable for road edge detection, where a combination of wavelets and Radon transform is needed. However, there are still some problems with this combination approach. First, a false maximum of the ridgelet coefficients can appear because of the step values in the Radon domain, which may lead to the identification of a false edge. Second, the support interval of each Radon slice is different, and the signal boundary extension for wavelet transformation must be treated distinctively. To solve these problems, this paper puts forward a newly revised parallel-beam Radon transform (RPRT) method, and the support intervals of the Radon slice are also given. A discrete ridgelet transform is performed and an algorithm to detect straight road edges is implemented. This approach is an improvement over other approaches as the geography and the radiometry of the road in high-resolution images are taken into account within the edge detection algorithm. The results show that, compared to the Canny operator and the edge extraction method based on segmentation, our algorithm can extract straight road edges from high-resolution remote sensing imagery more accurately and efficiently and can avoid cumbersome and complicated post-processing.

2. The ridgelet and the Radon transform

2.1 *The continuous ridgelet transform (CRIT)*

We start by briefly reviewing the ridgelet transform and showing its connections with other transforms in the continuous domain. Given an integrable bivariate function $f(x)$, its CRIT in $\Re^2$ is defined by (Candès 1998, Candès and Donoho 1999):

$$\mathrm{CRIT}_f(a,b,\theta) = \int_{\Re^2} \psi_{a,b,\theta}(x) f(x) \mathrm{d}x, \quad x = (x_1, x_2) \tag{1}$$

where a is a scale parameter, b a shift parameter, and the 2D ridgelets $\psi_{a,b,\theta}(x)$ are defined from a 1D wavelet-type function $\psi(x)$ as:

$$\psi_{a,b,\theta}(x) = a^{-1/2}\psi((x_1 \cos\theta + x_2 \sin\theta - b)/a) \tag{2}$$

where the function $\psi_{a,b,\theta}(x)$ is oriented at the angle θ and is constant along lines $x_1 \cos\theta + x_2 \sin\theta =$ constant. Figure 1 shows an example of a ridgelet function.

A basic tool for calculating ridgelet coefficients is to view ridgelet analysis as a wavelet analysis in the Radon domain. The Radon transform can be denoted as:

$$R_f(\theta,t) = \int_{\Re^2} f(x)\delta(x_1 \cos\theta + x_2 \sin\theta - t)\mathrm{d}x \tag{3}$$

where δ is the Dirac 'function', which is zero for every argument except 0 and its integral is one. In other words, R_f is the integral of f over the line $L_{t,\theta}$ defined by $x_1 \cos\theta + x_2 \sin\theta = t$ (see figure 2). For a more detailed description, see Beylkin (1987). In §2.2, we describe the Radon transform and its discretization algorithm.

The ridgelet transform is the application of a 1D wavelet transform to the slices (also referred to as projections) of the Radon transform:

$$\mathrm{CRIT}_f(a,b,\theta) = \int_R \psi_{a,b}(t) R_f(\theta,t)\mathrm{d}t \tag{4}$$

The Radon transform can efficiently convert singularities along straight lines to point singularities, and wavelets perform very well in handling point singularities, and therefore ridgelets are very effective in representing objects with singularities along

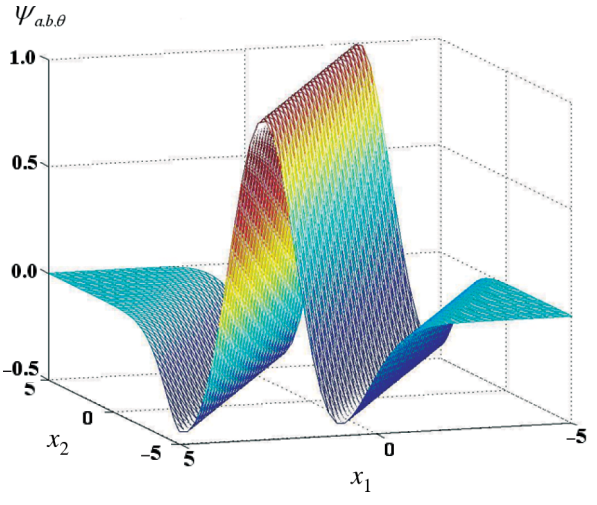

Figure 1. An example of the ridgelet function $\psi_{a,b,\theta}(x_1, x_2)$.

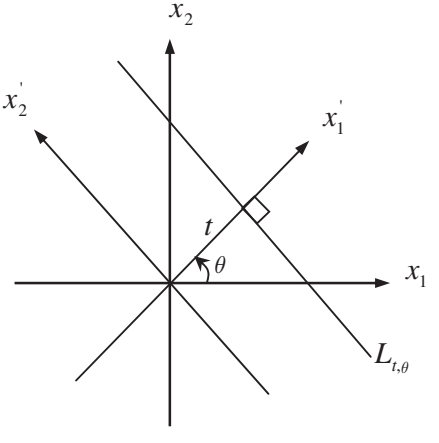

Figure 2. A Radon slice $R_f(\theta, t)$.

lines. In fact, ridgelets can be thought of as a way of concatenating 1D wavelets along lines. Hence, using ridgelets in image processing tasks is appealing because singularities are often joined together along edges or contours in images (Donoho and Vetterlin 2003, Carré and Andrès 2004).

2.2 *The discrete Radon transform*

As we have seen, a basic strategy for calculating the CRIT is first to compute the Radon transform R_f, and second to apply a 1D wavelet transform to the slices $R_f(\theta,:)$. The implementation of the discrete ridgelet transform can use the same principle. The discrete wavelet decomposition is easy to implement, but the discretization of the Radon transform is difficult to achieve (Carré and Andrès 2004) because of the

difficulty in obtaining discrete Radon transforms that can be reconstructed. However, this study considers only the detection of straight road edges, so the reconstruction of a discrete Radon transform is not considered. The only requirement is to accurately locate the position of the line through the discrete ridgelet transform, based on the discrete Radon transform. The projection method of the Radon transform can be divided into parallel-beam and fan-beam, and the latter can be converted to the former following a rebinning operation (George and Bresler 2007). The discrete Radon transform with parallel-beam projections is demonstrated in this paper. In §2.3 we present a revised version of the parallel-beam Radon transform that is suitable for straight road edge detection.

The 2D parallel-beam Radon transform of an image defined in (x_1, x_2) coordinate space is a set of projections of the image taken by integrating along the set of lines defined by $x_1 \cos\theta + x_2 \sin\theta = t$. Parameterized in this way, θ is the angle of the line with respect to the x_2-axis and t represents its distance from the origin O. An image in (x_1, x_2) space is thus transformed into Radon space (t, θ). A digital image $I(x_1, x_2)$ is an array of pixels, each representing the average grey level of a unit square in the image. A line integral along $x_1 \cos\theta + x_2 \sin\theta = t$ is approximated by a summation of the pixels lying in the 1-pixel-wide strip $t - 0.5 \leq x_1 \cos\theta + x_2 \sin\theta \leq t + 0.5$ (see figure 3).

As the strips have unit width, t can be restricted to integer values, and for an image with $N \times N$ pixels and a given θ, at most $\sqrt{2}N$ strips are needed. Angles are generally taken to be uniformly distributed between 0 and π (Brady and Yang 1992). However, for a fixed angle θ, some pixels are shared by two adjacent strips, so to improve the accuracy, each pixel in the image is first divided into four parts and each subdivision is projected separately, as shown in figure 4. Each pixel's contribution is split proportionally into the two nearest bins, according to the distance between the projected location and the bin centres. The Radon transform of an image is then the sum of the

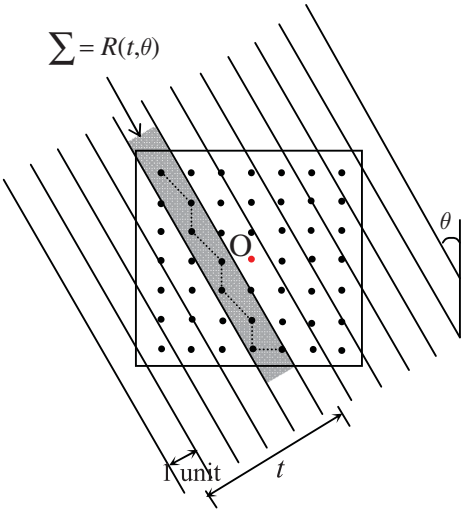

Figure 3. Representation of the set of strips for summation along a single direction, θ. One of the strips, shown in grey, represents a single Radon data point $R(t, \theta)$, and the solid dots represent the centre of pixels, where the red one, O, represents the origin of the image (Brady and Yang 1992).

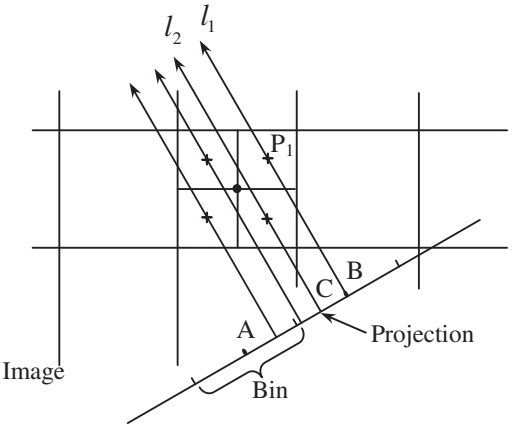

Figure 4. The Radon transform of an individual pixel. The solid dot represents the centre of a pixel and the four crosses represent the centres of the subpixels. A and B are respectively centre points of two bins, C is the projection of a subdivisional subpixel along l_2. The projection of subpixel P_1 along l_1 hits the centre point B of a bin (The Mathworks 1995a).

Radon transforms of each individual pixel according to the superposition principle (The Mathworks 1995a).

The above algorithm for the discrete Radon transform can accurately map singularities along lines to point singularities. However, for applications in edge detection, some problems still exist with this Radon transform. First, for the different projection angle θ, the length of the support interval (i.e. the length of the non-zero signal) of the Radon slice $R_f(\theta,:)$ varies. However, this must be known accurately for the wavelet border extension of the signal to be meaningful and for the detection of the maximum value of the wavelet coefficients' modulus. Second, the Radon transform will produce step values resulting from the different number of pixels in each strip, and these step values will result in a false maxima of the wavelet coefficients. In the next section we clarify these problems and provide the support interval of the Radon slice $R_f(\theta,:)$ as well as the revised discrete Radon transform suitable for our research purposes.

2.3 *Improved discrete Radon transform for road edge detection*

2.3.1 The support interval of $R_f(\theta,:)$. After the discrete Radon transform of the image, a 1D discrete wavelet transform (DWT) is applied to the Radon slice $R_f(\theta,:)$ to detect point singularities, where edges are probably located in the image. The basic algorithm for the DWT is based on convolution. As usual, when a convolution is performed on finite-length signals, border distortions arise. To deal with border distortions, the border should be treated differently from the other parts of the signal. Often it is preferable to use simple schemes based on signal extension on the boundaries (The Mathworks 1995b). However, for the square image of size $N \times N$ and the various angles of θ, the support interval of the Radon slice $R_f(\theta,:)$ varies (see figure 5). This results from the discretization algorithm of the Radon transform (see figure 6). We give the support interval $[-x'_1, x'_1]$ of $R_f(\theta,:)$ as the following, and with slight modification, the formula can be easily applied to a rectangular image.

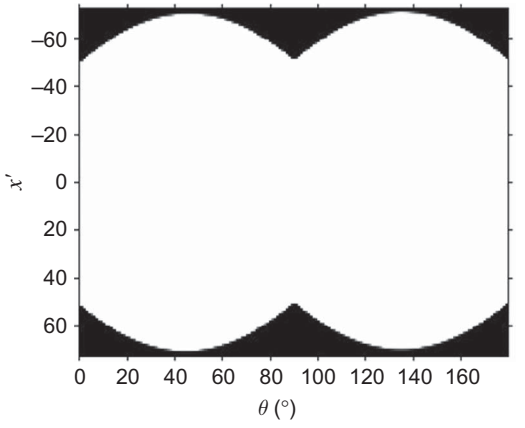

Figure 5. The Radon domain of a 100 × 100 image. The white part represents the support domain of the Radon transform and each column is the support interval of a Radon slice $R_f(\theta,:)$.

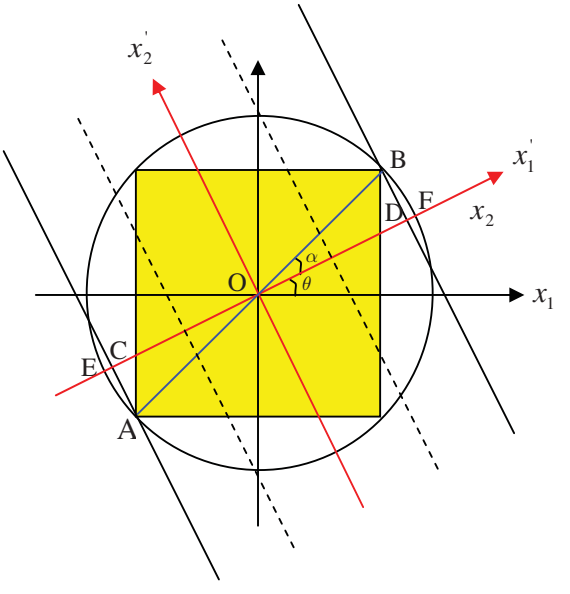

Figure 6. The computation of the support intervals of the Radon transform for an $N \times N$ square image.

$$[-x_1', x_1'] = \begin{cases} \left[-\frac{\sqrt{2}}{2}N\cos(\frac{\pi}{4}-\theta),\ \frac{\sqrt{2}}{2}N\cos(\frac{\pi}{4}-\theta)\right], & 0 \le \theta < \frac{\pi}{4} \\ \left[-\frac{\sqrt{2}}{2}N\cos(\theta-\frac{\pi}{4}),\ \frac{\sqrt{2}}{2}N\cos(\theta-\frac{\pi}{4})\right], & \frac{\pi}{4} \le \theta < \frac{\pi}{2} \\ \left[-\frac{\sqrt{2}}{2}N\cos(\frac{3\pi}{4}-\theta),\ \frac{\sqrt{2}}{2}N\cos(\frac{3\pi}{4}-\theta)\right], & \frac{\pi}{2} \le \theta < \frac{3\pi}{4} \\ \left[-\frac{\sqrt{2}}{2}N\cos(\theta-\frac{3\pi}{4}),\ \frac{\sqrt{2}}{2}N\cos(\theta-\frac{3\pi}{4})\right], & \frac{3\pi}{4} \le \theta < \pi \end{cases} \tag{5}$$

To avoid the influence of border distortions, we extend the support intervals of the Radon slices using smooth padding of order 1 according to equation (5). This method assumes that signals or images can be recovered outside their original support by a simple first-order derivative extrapolation: padding using a linear extension fit to the first two and last two values (The Mathworks 1995b). Then, after wavelet extension in the support intervals of the Radon slices, the maximum absolute values of the wavelet coefficients are detected.

2.3.2 The RPRT. It is obvious from the algorithm of the discrete Radon transform presented in §2.2 that the number of pixels in each strip will be different (see figure 3). This results in the value of the Radon slice $R_f(\theta,:)$ changing in steps, even if all pixels in the square image have the same values (figure 7(*a*)). We can obtain the number of the incremental pixels in each strip by geometric calculation from figure 8, in which $l_1, \ldots, l_m, \ldots, l_n, \ldots, l_k$ represent the centrelines of strips and λ (generally, $\lambda = 1$) denotes the width of the strip. The length difference (Δl) of each pair of adjacent strips, from l_1 to l_m and from l_k to l_n, intersected by the image borders can be computed as:

$$\Delta l = \lambda \tan\alpha + \lambda c\tan\alpha = \frac{2\lambda}{\sin 2\alpha} \tag{6}$$

where $\alpha = \begin{cases} \theta, & 0^\circ < \theta < 90^\circ \\ 180^\circ - \theta, & 90^\circ < \theta < 180^\circ \end{cases}$

Hence, for a given projected angle θ, Δl is constant, so that the ramp of AB in figure 7(*a*) should in theory be a straight line segment. The line segment BC is horizontal because the number of pixels in each two adjacent strips in figure 8 from l_m to l_n is fixed. The slope of AB (figure 7(*a*)) can be represented as:

$$S_{AB} = \frac{\Delta l}{\lambda} = \frac{2}{|\sin 2\theta|}, \tag{7}$$

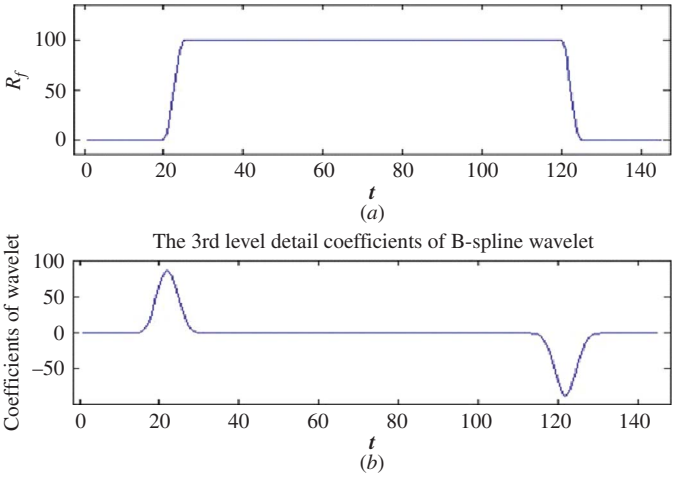

Figure 7. (*a*) The graph of the Radon slice $R_f(88^\circ,:)$ of an image with the values of all pixels being 1, and (*b*) its B-spline wavelet transform.

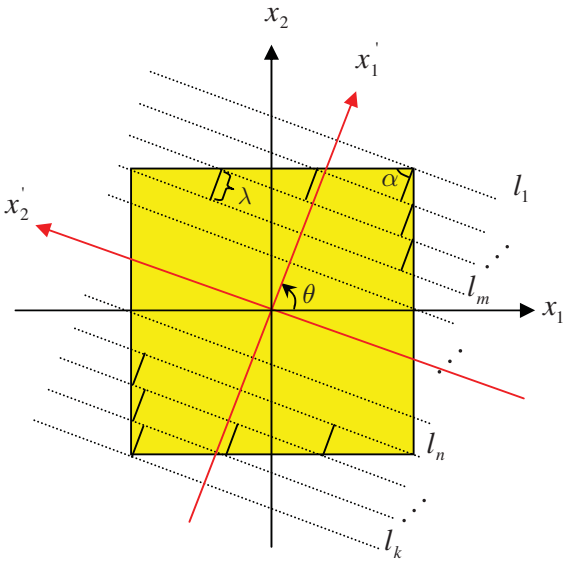

Figure 8. The scheme of the increment of the number of pixels in discrete Radon integrate strips, where $l_1, \ldots, l_m, \ldots, l_n, \ldots, l_k$ are the centrelines of strips.

Note that, when $\theta \to 0°$ or $\theta \to 90°$ or $\theta \to 180°$, $S_{AB} \to +\infty$; that is, the ramp AB becomes progressively steeper. As a result, this leads to the local maxima of a wavelet transform modulus (figure 7(*b*)), where false singularities might be expected. However, there are essentially no singularities at all in the original image. To avoid the detection of these false singularities, the Radon transform of the original image is revised by the Radon transform of the same size image with all pixel values being 1 unit, which can be denoted by

$$R_f^{\mathrm{R}}(i,j) = \frac{R_f(i,j)}{R_{\mathrm{I}}(i,j)} = \frac{\sum\limits_{\mathrm{P}_k \in S} w_k \mathrm{P}_k}{\sum\limits_{k} w_k} \tag{8}$$

where k denotes the number of pixels, $R_f^{\mathrm{R}}(i,j)$ is the (i,j) element of the revised Radon transform matrix of the original image; $R_f(i,j)$ is the (i,j) element of the Radon transform matrix of the original image; $R_{\mathrm{I}}(i,j)$ is the (i,j) element of the Radon transform matrix of the image with the pixel value being 1 unit; and S represents the strip corresponding to $R_f(i,j)$ (see figure 3). P_k denotes all subpixels within and shared by the strip S and w_k is the contribution of P_k to the bin of S (see figure 4). In fact, $R_f^{\mathrm{R}}(i,j)$ is equivalent to the harmonic average of all P_k in the strip S and w_k is the harmonic coefficient.

An image of the road model (figure 9) was used to test the method. Figure 10(*a*) is the graph of the Radon slice $R_f(89°,:)$ of figure 9, and figure 10(*b*) gives the wavelet detail coefficients of figure 10(*a*), that is the ridgelet coefficients with $\theta = 89°$ of figure 9. Figures 10(*c*) and 10(*d*) are graphs of the revised Radon slice $R_f^{\mathrm{R}}(89°,:)$ and its wavelet transform coefficients, respectively. By comparison, the revised Radon transform can effectively eliminate the false local maximum value of the ridgelet transform modulus, which might have been considered to indicate a road edge.

Figure 9. An image of the road model.

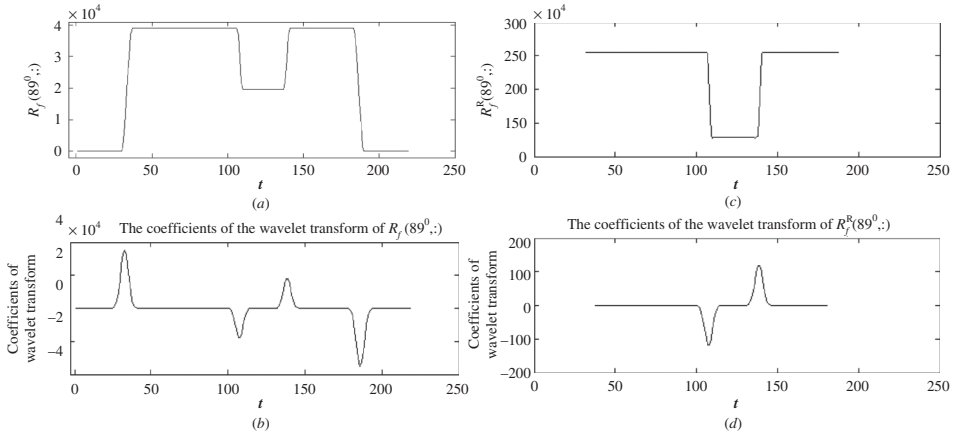

Figure 10. (*a*) The Radon slice $R_f(89°,:)$ of figure 9 and (*b*) its wavelet detail coefficients. (*c*) The revised Radon slice $R_f^{\mathrm{R}}(89°,:)$ and (*d*) its wavelet transform coefficients. Note that the valid Radon intervals are intercepted according to equation (5) in (*c*) and (*d*).

3. Straight road edge detection based on the ridgelet transform with RPRT

3.1 *Methods of straight road edge detection based on the ridgelet transform*

In high-resolution remote sensing imagery, road characteristics can be classified into five groups: geometrical, radiometric, topological, functional and contextual (Garnesson *et al*. 1990, Vosselman and Knecht 1995, Dal Poz *et al*. 2006). For road detection, geometrical and radiometrical characteristics are particularly important and the main ones include:

C1: Roads are elongated (geometry)
C2: Road edges are anti-parallel (geometry)
C3: The road surface often has a good contrast with the adjacent areas (radiometry)
C4: The road surface is usually homogeneous (radiometry)

These characteristics are the basis of road edge detection based on the ridgelet transform. Considering these characteristics and those of the RPRT discussed above, the algorithm for straight road edge detection is designed as follows, and the flowchart is given in figure 11:

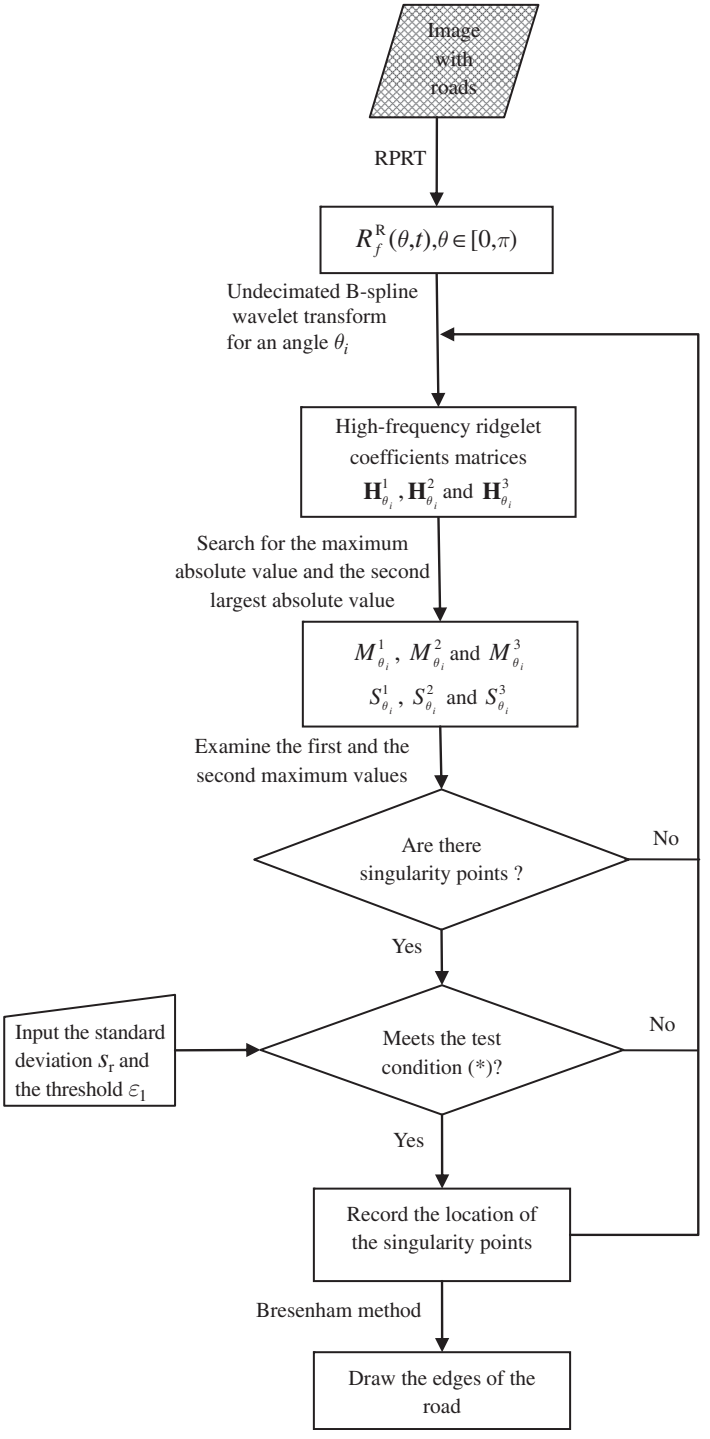

Figure 11. The flowchart of the proposed algorithm of straight road edge detection based on the ridgelet transform with RPRT.

(i) Make the RPRT mentioned in §2.3.2 into an input image, to calculate $R_f^{\mathrm{R}}(\theta, t), \theta \in [0, \pi)$;

(ii) Calculate the three-level undecimated B-spline wavelet transform, (which is widely used in edge detection), with the 1D extension of the signal (see §2.3.1) on the projection $R_f^{\mathrm{R}}(\theta_i, t)$ of the angle $\theta_i \in [0, \pi)$, to obtain the high-frequency ridgelet coefficients matrices $\mathbf{H}_{\theta_i}^1, \mathbf{H}_{\theta_i}^2, \mathbf{H}_{\theta_i}^3$. These are the multi-resolution representations of the ridgelet transform of the original image and are the basis for the MRA of singularities along lines.

(iii) Search for the maximum absolute value in the support intervals of the ridgelet coefficients $\mathbf{H}_{\theta_i}^1, \mathbf{H}_{\theta_i}^2$ and $\mathbf{H}_{\theta_i}^3$ (see §2.3.1), denoted by $M_{\theta_i}^1, M_{\theta_i}^2$ and $M_{\theta_i}^3$, and also the second largest absolute value, denoted by $S_{\theta_i}^1, S_{\theta_i}^2$ and $S_{\theta_i}^3$. If two or more identical maxima occur, then record and examine them. Examine the first maximum and the second maximum value detected in $\mathbf{H}_{\theta_i}^1, \mathbf{H}_{\theta_i}^2$ and $\mathbf{H}_{\theta_i}^3$ according to the multi-scale information (Mallat and Zhong 1992), and determine whether they are pairs of singularity points in $\mathbf{H}_{\theta_i}^1, \mathbf{H}_{\theta_i}^2$ and $\mathbf{H}_{\theta_i}^3$. If there are singularity points, then record their locations. Note that, according to the road's characteristics C1–C4 mentioned above, the locations of singularity points represented by the maximum value and the second maximum value are probably the two edges of a road. To avoid false identification, the following tests should also be performed: (*) Compute the standard deviation, denoted by s, of the greyscale of pixels between lines that the maximum value and the second maximum value represent in the original image. Let s_{r} be the real standard deviation of the greyscale of pixels of the road surface in the original image and $\varepsilon_1 > 0$ be the lower threshold, then if $|s - s_{\mathrm{r}}| < \varepsilon_1$, two edges of a road should exist, and the location parameters of the straight edges should be recorded.

(iv) For all angles in $R_f^{\mathrm{R}}(\theta, t)$, repeat steps (ii) and (iii).

(v) Create an image matrix $\mathbf{B}$, with all pixel values being 0, with the same size as the original image and use the Bresenham method (Bresenham 1965) to draw the edges of the road that were located by step (iv) in $\mathbf{B}$.

Some parameters in the above algorithm need to be estimated and input. These may be easily obtained in the pre-processing. In (*), the standard deviation s_{r} and the threshold ε_1 can be obtained by sampling from the road region of the original image with interactive image processing software (e.g. Envi 4.3). The standard deviation reflects the homogeneity characteristic (C4) that is generally assumed for roads. It is in essence a consistency check between the standard deviation of the grey level of the expected road surface and that of the real road surface as the spectral characteristics of road surfaces may vary because of the differences in the road surface materials (e.g. asphalt or concrete). This input ensures the accuracy of the edge detection by sampling from the road region of the original image and comparing it to the spectral value of the detected road surface.

3.2 *Accuracy assessment*

Pratt's figure of merit (FOM) (Pratt 1978) was used to assess the accuracy of the road edge detection in our experiment. To test the effectiveness of our algorithm:

$$\mathrm{FOM} = \frac{1}{\max(I_{\mathrm{A}}, I_{\mathrm{I}})} \sum_{i=1}^{I_{\mathrm{A}}} \frac{1}{1 + ad_i^2} \tag{9}$$

where I_A and I_I represent the number of actual edge map (extracted by the edge detection algorithm) and ideal edge map (extracted manually) points here. a is a scaling constant to penalize edges that are localized but offset from the true position, and d_i is the separation distance of an actual edge point normal to a line of ideal edge points. The rating factor FOM is normalized and ranges from 0 to 1, where 1 indicates a perfectly detected edge. Normalization by the maximum of the actual and ideal number of edge points ensures a penalty for smeared or fragmented edges (Pratt 2001). Thus the FOM calculates the deviation of the detected edge with respect to an ideal edge map.

4. Results and discussion

To test the effectiveness of the algorithm, we cut out a square area containing a known straight road, size 192×192 pixels, from band 3 of a QuickBird image of Changchun city with a pixel resolution of 2.4 m (figure 12(*a*)). We use Envi4.3 to compute the standard deviation of the greyscale of pixels of the road surface, $s_r = 19.5131$, and set $\varepsilon_1 = 5$. The RPRT and the results of the straight road edge extraction are shown in figures 12(*b*) and 12(*c*). By contrast, figures 12(*d*)–12(*g*) give the edge detection results of Sobel, Roberts and Canny operators as programmed in the commercially available software Matlab 7.0 (The Mathworks Inc. 2004).

It is clear from figures 12(*e*) and 12(*f*) that the Canny edge operator, which is equivalent to finding the local maxima of a wavelet transform modulus (Mallat and Zhong 1992), gives better visual detection results than the Sobel and Roberts operators. However, for the purpose of road edge extraction, overdetection by the Canny operator is serious as it also detects edge pixels of buildings. To eliminate these non-road edges we adjusted the threshold progressively until the best road-edge detection result was achieved, as shown in figure 12(*g*), with a sensitivity threshold of [0.55, 0.58]. Most of the non-road edges are removed but the detection of the edge of the road becomes discontinuous.

Visual inspection of the results in figure 12(*c*) reveals considerable success using the algorithm proposed here. The results of the quantitative accuracy assessment (equation (9)) validate this impression, on the basis of the manually plotted reference data. In figures 12(*c*)–12(*g*), FOM values are, respectively, 0.8960, 0.0562, 0.0514, 0.0329 and 0.1806, where the parameter a is taken as 0.4. The edge detection results based on our algorithm obtain the highest FOM score. Note that we only assess the edge detection of the single object of interest (the road), so non-road edge points are considered as noise. Although the road edges detected by the Canny operator are more continuous than those detected by the Sobel and Roberts operators, more non-road edge points are also detected, so the FOM score of the Canny operator is much less than those of the Sobel and Roberts operators. After the threshold is adjusted, most of non-road edge points detected by the Canny operator are eliminated (as shown in figure 12(*g*)). In this case, the FOM score increases slightly, but is still not high because the edge of road is more discontinuous.

The edge detection method developed in this paper is object based and other classical detectors are pixel based. Therefore, it is appropriate that the FOM value calculation for other methods should be based on the edge pixels related to the longest road only. The new FOM scores, denoted by New-FOM, of these edge detectors in figures 12(*d*)–12(*g*) are, respectively, 0.62105, 0.64381, 0.55976 and 0.54412. These values are still low compared to the FOM value of 0.8960 for our method.

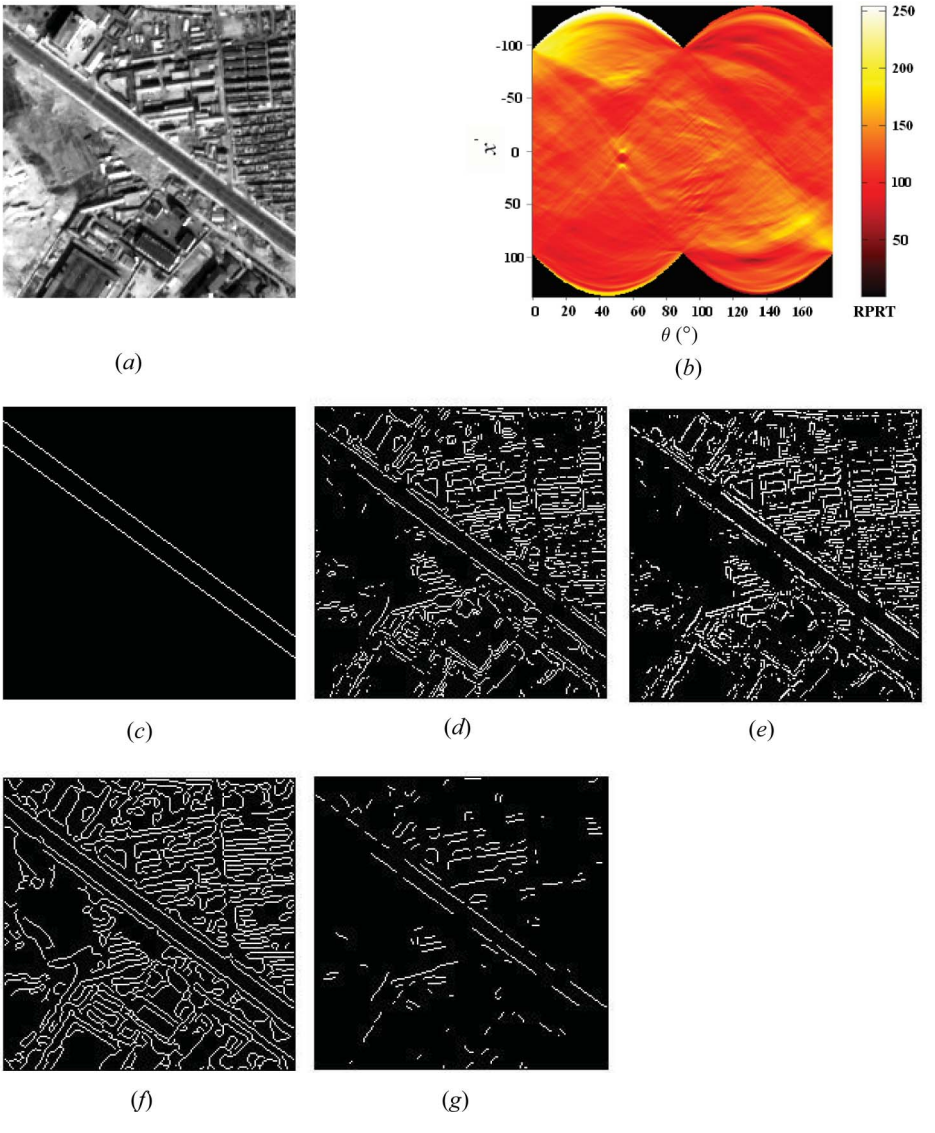

Figure 12. (*a*) The original image; (*b*) revised parallel-beam radon transform (RPRT) of the image; (*c*) the detection result with the algorithm proposed in this paper, running time = 0.8 s; (*d*) Sobel operator detecting result with threshold = 0.17, running time = 0.4 s; (*e*) Roberts operator detection result with threshold = 0.23; running time = 0.3 s; (*f*) Canny operator detection result with default threshold = [0.125, 0.3125], running time = 0.2 s; (*g*) Canny operator detecting result with threshold = [0.55, 0.58] to eliminate non-road edges.

For further comparison, another road edge map based on a segmentation and classification method (a non-edge detection-based method) was also constructed and compared. Figure 13(*a*) is the classification result of the original image (figure 12(*a*)) using the unsupervised *k*-mean classification method. Figures 13(*b*) and 13(*c*) (the road edge map) are the segmentation map and the edge extraction map after classification, respectively. It can be seen that there are many discontinuities in the road

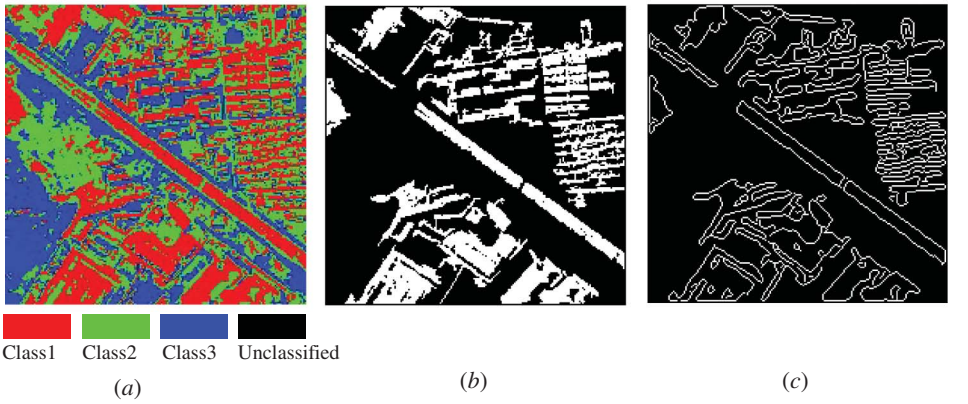

Figure 13. (*a*) *k*-means classification for the road image. (*b*) The segmentation result of the classification image and (*c*) the road edge extraction.

surface and non-road features (buildings) in the map. The FOM and New-FOM scores are also small (0.0331, 0.55813), lower than those of the Canny detection result (see figure 12(*d*)) and of the detection result of our proposed algorithm (figure 12(*c*)).

To validate the detection ability of the algorithm for the other road scenes in the image, the experiment was also performed for the other two IKONOS Pan images, 234 × 316 and 234 × 512 pixel size, with cross-roads and almost parallel roads (see figures 14(*a*) and 14(*d*)). For the scene with the road crossing, the algorithm can detect the road edge lines accurately but the lines intersect at the crossing (figure 14(*b*)). However, simple post-processing can delete the intersecting line segments and the last result is shown in figure 14(*c*) (the FOM score is 0.9012). If there are two or more almost parallel roads in the image (e.g. figure 14(*d*)), there will be more than two local maximum values at some angle $\theta_i \in [0, \pi)$ in the ridgelet coefficients. Then the test condition (*) will play an important role in confirming the road edges. If the standard deviation of the greyscale of the pixels of the road surface between the two local maximum values cannot meet the condition (*), these two edges cannot be those of the same road. In the experiment we obtained the standard deviation of the greyscale of pixels of the road surface using Envi4.3, $s_r = 14.2093$, and set $\varepsilon_1 = 4$. Figure 14(*e*) gives the detection result (the FOM score is 0.8813).

The above experiment results were obtained on a PC with Pentium IV 2.4 GHz CPU running under Matlab 7.0, and the processing times are given respectively in the notes of figures 12 and 14. The results show that our algorithm runs slightly slower than the classical edge detectors (Canny, Sobel and Roberts), but with the simplified post-processing and the better detection results, the processing times are acceptable.

In general, a large amount of post-processing work is required after detection with classical per-pixel edge detection operators or using a segmentation and classification method. This is due to road edge over- or underdetection. In this paper the road edge detection method based on the ridgelet transform incorporates the road geometry and radiometry characteristics, and can accurately locate and extract the straight edges of the road. Moreover, we agree with Hou *et al.* (2003) that the length of the object edge being examined can be extracted directly using a ridgelet transform, which the other edge detection operators cannot achieve.

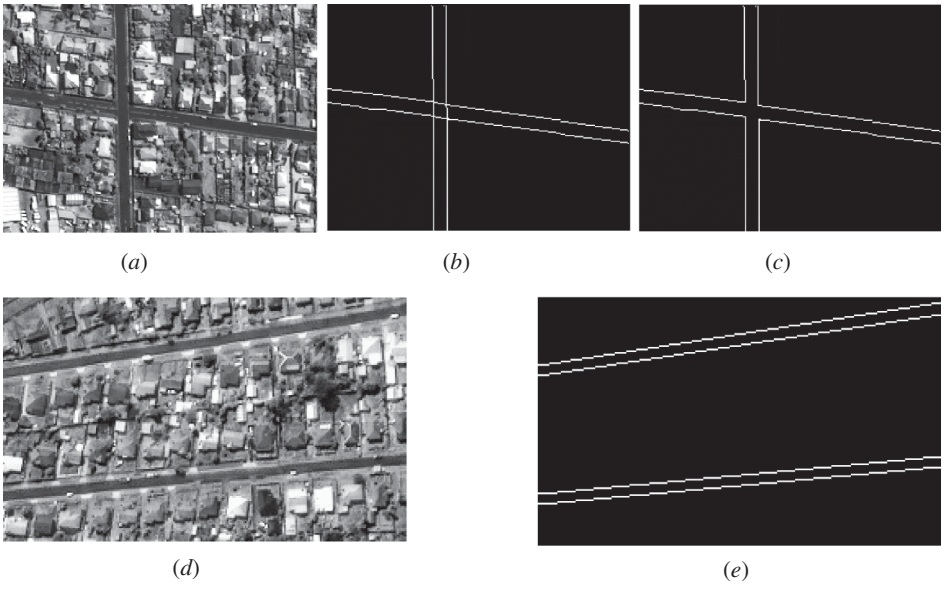

Figure 14. (*a*) An IKONOS image with cross-roads; (*b*) the detection result by the proposed method, running time = 2.1 s; and (*c*) the result after post-processing. (*d*) An IKONOS image with almost parallel roads and (*e*) the detection result, running time = 2.8 s.

Because of the character of the parallel-beam Radon transform itself, for the roads that do not span the entire image our algorithm is unable to locate the end-point of the road edge. A new strategy (e.g. Cardoso 1999) and a new Radon transform (e.g. a localized Radon transform; Copeland *et al.* (1995)) must therefore be designed and introduced into the road edge detection algorithm. These will be developed in our future work.

5. Conclusion

In this paper, we analysed the principle of parallel-beam Radon transform,and proposed the RPRT, which solves the problem of the false maximum of the coefficients in the Radon domain. The support interval of each Radon slice is also derived, which helps to accurately extend the signal boundary of the Radon slice for wavelet transformation. Hence, a more effective framework of the ridgelet transform is established by combining the RPRT and wavelets.

The ridgelet transform can deal efficiently with linear singularities in two dimensions. The general concept is to map linear singularities in the spatial domain to point singularities in the Radon domain, and then deal with the resulting point singularities using a wavelet system. The Radon transform can change higher-dimensional singularities into point singularities, and the wavelet is the optimal basis for representing point singularities. The framework of the ridgelet analysis can be constructed efficiently in combination with the Radon transform and the wavelet transform (Hou *et al.* 2003). With the character of multi-orientation, which is lacking in wavelet transforms (Donoho 2000, Jiao *et al.* 2005), the ridgelet transform based on the RPRT proposed in this paper can capture linear singularities efficiently and

accurately. The characteristics of objects being detected, such as geometry and radiometry, can be used when using the ridgelet transform and this enhances the performance of this algorithm in automatic pattern recognition.

The newly constructed ridgelet transform, combined with radiometric and geometric characteristics, was successfully applied in road edge detection in high-resolution imagery. Our experiments show that, with less over- or underdetection, the accuracy of road edge detection with our approach is higher than that of traditional edge detection operators and is also better than the *k*-mean classification method (non-edge detection-based road classification method). For the other scenes included in the image (e.g. cross-roads and almost parallel roads in the image), our algorithm can also detect the road edges accurately.

Although only the algorithm for detecting straight road edges is discussed in this paper, it is also possible to design an algorithm based on the RPRT and ridgelet analysis to adaptively detect the edges of crossing segments (Liu and Jiao 2004, Tóth and Barsi 2005, Tang and Cheng 2006). Furthermore, edge detection for a curved road edge could make use of a curvelet, the further expansion of a ridgelet (Candès and Donoho 2005*a*,*b*, Nencini *et al.* 2007). This will be included in our future work.

Acknowledgements

We thank the three anonymous referees for their valuable comments, which led to a significant improvement in this paper. This research was supported by the Knowledge Innovation Programme of the Chinese Academy of Sciences (No. KZCX3-SW-356) and the Science Data Sharing Project of the Ministry of Science and Technology of China (No. 2006DKA32300-16).

References

Beylkin, G., 1987, Discrete Radon transform. *IEEE Transactions on Acoustics, Speech and Signal Processing*, **35**, pp. 162–172.

Brady, M.L. and Yang, W., 1992, Fast parallel discrete approximation algorithms for the Radon transform. In *Proceedings of the ACM Symposium on Parallel Algorithms and Architectures, SPAA*, 1992, San Diego, CA, pp. 91–99 (New York, USA:ACM).

Bresenham, J.E., 1965, Algorithms for computer control of a digital plotter. *IBM Systems Journal*, **4**, pp. 25–33.

Candès, E.J., 1998, Ridgelets: theory and applications. PhD thesis, Department of Statistics, Stanford University, CA.

Candès, E.J. and Donoho, D.L., 1999, Ridgelet: a key to high-dimensional intermittency. *Philosophical Transactions of the Royal Society of London, Series A*, **357**, pp. 2495–2509.

Candès, E.J. and Donoho, D.L., 2005*a*, Continuous curvelet transform: I. Resolution of the wavefront set. *Applied and Computational Harmonic Analysis*, **19**, pp. 162–197.

Candès, E.J. and Donoho, D.L., 2005*b*, Continuous curvelet transform: II. Discretization and frames. *Applied and Computational Harmonic Analysis*, **19**, pp. 198–222.

Cardoso, L.A., 1999, Computer-aided recognition of man-made structures in aerial photographs. Master's thesis, Naval Postgraduate School, Monterey, CA.

Carré, P. and Andrès, E., 2004, Discrete analytical ridgelet transform. *Signal Processing*, **84**, pp. 2165–2173.

Chiang, T.-Y., Hsieh, Y.-H. and Lau, W., 2001, *Automatic Road Extraction from Aerial Images.* Available online at http://scien.stanford.edu/class/ee368/projects2001/dropbox/project10/main.html.

Copeland, A.C., Ravichandran, G. and Trivedi, M.M., 1995, Localized Radon transform-based detection of ship wakes in SAR images. *IEEE Transactions on Geoscience and Remote Sensing*, **33**, pp. 35–45.

COULOIGNER, I. and RANCHIN, T., 2000, Mapping of urban areas: a multiresolution modeling approach for semi-automatic extraction of streets. *Photogrammetric Engineering and Remote Sensing*, **66**, pp. 867–874.

DAL POZ, A.P., GYFTAKIS, S. and AGOURIS, P., 2000, Semiautomatic road extraction: comparison of methodologies and experiments. In *2000 ASPRS Annual Conference*, Washington, DC, USA. Available on CD-ROM.

DAL POZ, A.P., ZANIN, R.B. and DO VALE, G.M., 2006, Automated extraction of road network from medium- and high-resolution images. *Pattern Recognition and Image Analysis*, **16**, pp. 239–248.

DONOHO, D.L., 2000, Orthonormal ridgelets and linear singularities. *SIAM Journal on Mathematical Analysis*, **3**, pp. 1062–1099.

DONOHO, M.N. and VETTERLIN, M., 2003, The finite ridgelet transform for image representation. *IEEE Transactions on Image Processing*, **12**, pp. 16–28.

DU, G. and YEO, T.S., 2004, A novel Radon transform-based method for ship wake detection. In *Geoscience and Remote Sensing Symposium, 2004. IGARSS '04. Proceedings. 2004 IEEE International*, vol. 5, pp. 3069–3072.

GARNESSON, PH., GIRAUDON, G. and MONTESINOS, PH., 1990, An image analysis system, application for aerial imagery interpretation. In *Proceedings of the 10th International Conference on Pattern Recognition, ICPR*, 16–21 June 1990, Atlantic City, NJ, vol. 1, pp. 210–212.

GEORGE, A.K. and BRESLER, Y., 2007, Shear-based fast hierarchical backprojection for parallel-beam tomography. *IEEE Transactions on Medical Imaging*, **26**, pp. 317–334.

GUAN, L., WANG, P., HUANG, F. and LIU, X., 2006, Study on urban house information extraction automatically from QuickBird images based on space semantic model. In *IEEE International Conference on Geoscience and Remote Sensing Symposium, IGARSS*, July 2006, Denver, CO, pp. 1501–1504.

HINZ, S., BAUMGARTNER, A., MAYER, H., WIEDEMANN, C. and EBNER, H., 2001, Road extraction focussing on urban areas. In *Automatic Extraction of Man-Made Objects from Aerial and Space Images (III)*, E. Baltsavias, A. Gruen and L. Van Gool (Eds.), pp. 255–265 (Rotterdam: Balkema).

HOU, B., LIU, F. and JIAO, L.C., 2003, Linear feature detection based on ridgelet. *Science in China, Series E*, **46**, pp. 141–152.

JIAO, L.C., TAN, S. and LIU, F., 2005, Ridgelet theory from ridgelet transform to curvelet. *Chinese Journal of Engineering Mathematics*, **22**, pp. 761–773.

LAPTEV, I., MAYER, H., LINDEBERG, T., ECKSTEIN, W., STEGER, C. and BAUMGARTNER, A., 2000, Automatic extraction of roads from aerial images based on scale space and snakes. *Machine Vision and Applications*, **12**, pp. 23–31.

LI, D.R. and SHAO, J.L., 1994, The wavelet and its application in image edge detection. *ISPRS Journal of Photogrammetry and Remote Sensing*, **3**, pp. 4–11.

LIU, K. and JIAO, L.C., 2004, Adaptive curved feature detection based on ridgelet. In *International Conference on Image Analysis and Recognition, ICIAR*, 29 September–1 October 2004, Porto, Portugal, pp. 487–494.

MALLAT, S. and ZHONG, S., 1992, Characterization of signal from multiscale edge. *IEEE Transactions on Pattern Analysis and Machine Intelligence*, **14**, pp. 710–732.

MENA, J.B., 2003, State of the art on automatic road extraction for GIS update: a novel classification. *Pattern Recognition Letters*, **24**, pp. 3037–3058.

NENCINI, F., GARZELLI, A., BARONTI, S. and ALPARONE, L., 2007, Remote sensing image fusion using the curvelet transform. *Information Fusion*, **8**, pp. 143–156.

NEVATIA, R. and BABU, K.R., 1980, Linear feature extraction and description. *Computer Graphics and Image Processing*, **13**, pp. 257–269.

OLIVEIRA, H. and CAEIRO, J.J., 2000, Automatic search of roads in digital cartography [in Portuguese]. *Actas da II Conferencia Nacional de Cartografia e Geodesia, Lisboa*.

PRATT, W.K., 1978, *Digital Image Processing,* pp. 497–499 (New York: John Wiley & Sons, Inc.).

PRATT, W.K., 2001, *Digital Image Processing*, 3rd edn pp. 490–492 (New York: John Wiley & Sons, Inc.).

RADON, J., 1917, On the determination of functions from their integrals along certain manifolds [in German]. *Mathematish-Phyikalishe Klasse*, **69**, pp. 262–277.

RAMOS TERRADES, O. and VALVENY, E., 2006, A new use of the ridgelets transform for describing linear singularities in images. *Pattern Recognition Letters*, **27**, pp. 587–596.

SCHMEELK, J., 2005, Wavelet transforms and edge detectors on digital images. *Mathematical and Computer Modelling*, **41**, pp. 1469–1478.

THE MATHWORKS, INC., 1995a, *Image Processing Toolbox User's Guide*. Available online at http://www.mathworks.com/access/helpdesk/help/toolbox/images/.

THE MATHWORKS, INC., 1995b, *Wavelet Toolbox User's Guide*. Available online at http://www.mathworks.com/access/helpdesk/help/toolbox/wavelet/waveleta.html.

TOUZI, R., LOPES, A. and BOUQUET, P., 1988, A statistical and geometrical edge detector for SAR images. *IEEE Transactions on Geoscience and Remote Sensing*, **26**, pp. 764–773.

TANG, M. and CHENG, L.Z., 2006, Edge detection based on adaptive ridgelet transform. *Computer Applications*, **26**, pp. 2713–2715.

TÓTH, Z. and BARSI, A., 2005, Analyzing road junctions by geometric transformations. In *Proceedings of ISPRS Hannover Workshop on High-Resolution Earth Imaging for Geospatial Information*, 17–20 May 2005, Hannover, Germany. Available online at: http://www.isprs.org/publications/related/hannover05/paper/papers.htm.

VOSSELMAN, G. and KNECHT, J., 1995, Road tracing by profile matching and Kalman filtering. In *Proceedings of the Workshop on Automatic Extraction of Man-Made Objects from Aerial and Space Images* pp. 265–274 (Switzerland: Birkhauser Verlag).

ZHANG, Q. and COULOIGNER, I., 2007, Accurate centerline detection and line width estimation of thick lines using the Radon transform. *IEEE Transactions on Image Processing*, **16**, pp. 310–316.

Copyright of International Journal of Remote Sensing is the property of Taylor & Francis Ltd and its content may not be copied or emailed to multiple sites or posted to a listserv without the copyright holder's express written permission. However, users may print, download, or email articles for individual use.